Applied Thermal Engineering 137 (2018) 319–328

Contents lists available at ScienceDirect

Applied Thermal Engineering

journal homepage: www.elsevier.com/locate/apthermeng

Research Paper

Application of large underground seasonal thermal energy storage in district heating system: A model-based energy performance assessment of a pilot system in Chifeng, China

Luyi Xu[a,*], J. Ignacio Torrens[a,c], Fang Guo[b], Xudong Yang[b], Jan L.M. Hensen[a]

[a] Department of the Built Environment, Eindhoven University of Technology, De Rondom 70, 5612 AP Eindhoven, The Netherlands
[b] Department of Building Science and Technology, Tsinghua University, 100084 Beijing, China
[c] Sustainable Construction Division, TECNALIA, C/Geldo, Edificio 700, 48160 Derio, Bizkaia, Spain

ARTICLE INFO

Keywords:
Building performance simulation
District heating
Industrial waste heat
Modelica
Seasonal thermal energy storage
Solar thermal collectors

ABSTRACT

Seasonal thermal energy storage (STES) technology is a proven solution to resolve the seasonal discrepancy between heating energy generation from renewables and building heating demands. This research focuses on the performance assessment of district heating (DH) systems powered by low-grade energy sources with large-scale, high temperature underground STES technology. A pilot DH system, located in Chifeng, China that integrates a 0.5 million m^3 borehole thermal energy storage system, an on-site solar thermal plant and excess heat from a copper plant is presented. The research in this paper adopts a model-based approach using Modelica to analyze the energy performance of the STES for two district heating system configurations. Several performance indicators such as the extraction heat, the injection heat and the storage coefficient are selected to assess the STES system performance. Results show that a lower STES discharge temperature leads to a better energy performance. A sensitivity analysis of the site properties illustrates that the thermal conductivity of soil is the most influential parameter on the STES system performance. The long-term performance of the STES is also discussed and a shorter stabilization time between one and two years could be achieved by discharging the STES at a lower temperature.

1. The fundamental idea of STES in district heating systems

1.1. Status of the heating market in China

The buildings sector is responsible for almost one-third of the global final energy demand. The situation in China is particularly acute. In 2010, China replaced the United States as the largest energy consumer in the world. With its rapidly growing economy and improvement in living standards, China is witnessing a rapid expansion of its building industry, resulting in ever increasing energy demands. If building heating systems in China continue to be supplied by fossil fuels, China will suffer from increasing greenhouse gas emissions, and will miss the opportunity to gain economic benefits from alternative energy sources.

The Chinese government developed a national heating reform to improve building energy efficiency. As part of an effective approach to improving total energy efficiency, developments of district heating systems have grown exponentially since 2005 [1]. In addition, the government has promoted a series of standards and plans to adjust energy structure. The 13th Renewable Energy Development Five Year Plan (13th FYP) has set a target of increasing the share of non-fossil energy in the total primary energy consumption to 15% by 2020 and to 20% by 2030. One of the key objectives is to use renewable energy sources to substitute for 150 million metric tons coal equivalent energy from fossil fuels in the heating and domestic sector [2]. The plan provides opportunities for the development of 4th generation district heating systems, which aim to include more types of renewable energy sources (RES) and to recover industrial waste heat as supply sources [3].

As for the status of district heating in China, China now ranks second only after Russia in installed capacity of district heating systems. However, district heating systems in China still typically rely on coal and gas to generate heat. Nonetheless, the demand for district heating in China is expected to significantly increase in the near future. This is mainly due to the growing demand for DH systems in urban areas of Southern China, especially in urbanized big cities near the east seashore such as Shanghai, Hangzhou, Nanjing, etc. [4]. This means that it is essential to evaluate alternative generation sources.

In addition to the desire to limit the use of fossil fuels, the efficiency

* Corresponding author.
E-mail address: l.xu2@tue.nl (L. Xu).

https://doi.org/10.1016/j.applthermaleng.2018.03.047
Received 1 November 2017; Received in revised form 27 February 2018; Accepted 14 March 2018
Available online 21 March 2018

Nomenclature

c	specific heat capacity, J/(kg·K)
C	thermal capacitance, J/K
d	density, kg/m^3
g	grout
IC	influence coefficient
IP	value of input parameter
k	thermal conductivity, W/(m·K)
mf	mass flow rate, kg/s
OP	value of output parameter
Q	heat gain, kW
R	thermal resistance, K/W
S	storage coefficient
s	soil
T	air temperature, ˚C
t	time, year
B	baseline
dem	demand
ex	external
ext	extraction
in	indoor
inj	injection
inl	inlet
int	internal
r	return
ref	reference
s	stable

of heat distribution in China is another issue. District heating systems in China were originally based on steam for delivering heat, but have increasingly transitioned to hot water to improve the efficiency of heat distribution. However, the associated heat distribution losses in China are much higher than in western countries. These losses account for 30% of the total heat supply in China, while in Sweden they account for only 6–15% [5]. This difference can be caused by higher DH supply temperature applied in China with a range of 115–130 ˚C [6] while the national average supply temperature in Sweden and Denmark was 86.0 ˚C and 77.6 ˚C respectively [7]. In addition, hydraulic imbalances and leakage in distribution pipes in Chinese DH systems further aggravated the heat distribution losses.

1.2. The essential role of STES in 4th generation district heating systems

Large variations in outdoor temperatures between summer and winter generate large heat load variations over the year. However, the varied heat load is generally not well matched with heating sources in the 4th generation district heating systems. Take industrial waste heat as an example; the amount of recovered heat depends on the industrial process and it is very likely to be relatively constant all year round. In this case, a significant amount of heat will be wasted during the summer season when there is minimal heating demand. This mismatch represents an opportunity for seasonal thermal energy storage (STES) systems. The systems are usually coupled either individually, or in combination with large-scale solar thermal plants, combined heat and power (CHP) or industrial waste heat to compensate for the rather low heat demand during summer and large heat demand in winter. STES systems can be charged during the summer, for instance by solar thermal production, and retain the energy for later use during the colder winter months [8].

1.3. Underground STES in district heating systems

Unlike other components in district heating systems, STES is not a stand-alone component. STES cannot produce energy by itself. Therefore, the energy performance of STES mainly depends on its own operating condition and on the interaction with other system components. The amount of heat and temperature of the heat carriers during charging and discharging periods greatly influences the storage efficiency. Moreover, and especially for underground STES, energy performance is also significantly influenced by geographic characteristics and site properties, e.g. thermal conductivity of the soil, underground water, flow velocity, outdoor temperature etc. The relationship between the system fluid temperatures and the ground temperatures is strongly dependent on ground thermal conductivity. In the long term, the ground density and specific heat capacity also have an effect. Take borehole thermal energy storage as an example, the borehole thermal resistance defines the steady-state relationship between the system fluid temperature and the temperature at the borehole wall. The resistance depends on the dimension of the borehole thermal energy storage and the thermal properties of the grout material. These variations influence the specific power of the borehole heat exchanger (in watt per meter of borehole length), which varies from 10 W/m to 120 W/m according to information extracted from borehole-STES projects from the US and European countries [9]. In order to store and extract heat seasonally and to reduce the investment cost, it is beneficial to build underground STES on a relatively large scale with a minimal volume of 20,000 m^3. Large scale STES projects are also more efficient in terms of both technical feasibility and financial viability. Large scale STES usually takes two to five years to reach ‘design’ operating conditions [10]. Therefore, long-term performance assessment is required, which makes the design and performance analysis of underground STES systems a considerable challenge. As previously stated, representing the dynamic interaction with other DH system components is as well crucial. Then in this respect, computational simulation is possibly the only way to assist in the design process under the challenges.

Various models have been reported to represent the performance of different types of underground STES. This section presents an overview of underground STES models specifically used for borehole thermal energy storage. Borehole thermal energy storage consists of a number of borehole heat exchangers, which transfer heat between heat carrier and the soil. Several borehole heat exchanger models are available. The most widely used is the analytical g-function model, originally developed by Eskilson [11]. The g-function converts the temperature response of the borehole field into a dimensionless form in response to a step heat input. It is only valid for time-steps longer than three to six hours for a typical borehole, which is larger than the normal time-step (one hour) in building performance simulation. The original g-function model has been further improved by Yavuzturk and Spitler [12] to manage short time steps and also to take into consideration the thermal capacitance and resistance of individual borehole elements. Transient System Simulation Tool (TRNSYS) already implemented several borehole field models. The most common model is the Duct Ground Heat Storage Model (DST). A limitation of the model is that it is only applicable for cylinder-shaped Borehole Thermal Energy Storage (BTES) with vertical symmetry axis and uniformly placed ducts [13]. It adopts a steady-flux regime which considers a constant heat injection/extraction rate. Thus, the DST model ignores the dynamics of the heat exchange between the borehole wall and the heat carrier fluid. It also overestimates the long-term temperature response [14]. In order to simulate user-defined borehole configurations and obtain short-term and long-term accuracy for yearly-based simulations, Picard and Helsen [14] developed a hybrid step-response model (HSRM) for borehole field heat exchangers in Modelica©. Another advantage of the HSRM model over other models is the possibility of being implemented in multiple borehole simulations. Based on the summarized challenges in assessing the energy performance of underground STES, the HSRM model covers

most of the requirements, and therefore is adopted in the presented case study.

The amount of energy injected in/extracted from the underground STES in different time scales is commonly used to quantify the energy performance of the underground STES [9,15]. In addition, storage coefficient S can be calculated to represent the relationship between extracted heat Q_{ext} and injected heat Q_{inj} [16]. Heat losses [17] from underground thermal energy storage, excluding Aquifer Thermal Energy Storage (ATES), are mainly associated with conductive heat transfers from the storage volume to the surrounding soil. For a known storage volume, the heat exchange surface area between the heat storing volume and the outside environment becomes an alternative indicator for heat losses.

Another indirect indicator to describe heat losses for underground STES is a time-related performance indicator, the stabilization time t_s, which defines the start-up time after construction to reach normal operating conditions. During the stabilization period, heat carrier raises the temperature of the surrounding ground, therefore, heat loss is higher than at the normal operation period. Thus, an underground STES with a shorter stabilization period has a better energy performance.

To summarize, the 4th generation district heating system is a promising technology to promote the energy transition in China. Since in 4th generation district heating system a huge amount of heat is available when the heating demand is relatively low, normally in warm seasons, there is a clear opportunity to implement STES in DH system. However, the transient thermal behavior plays an essential role in the short and long-term thermal performance of STES systems, especially for underground STES. It is necessary to conduct detailed analyses to understand the thermal behavior of underground STES systems and to assess their energy performance. The research in this paper presents a model-based method that supports energy performance assessments of underground STES in district heating system. This method is demonstrated using a pilot case study in Chifeng, China.

2. The concept of STES with low-grade heat in district heating systems– a pilot case study in Chifeng, China

A copper plant located in the south of Chifeng City, Inner Mongolia, China (42°15′N 118°53′E) possesses a significant amount of industrial waste heat as a result of its industrial processes. This excess heat has a total power of 100 MW and is serving a 0.2 million m^2 residential area as part of the Chifeng City district heating network, and the office buildings of the copper plant since 2013. According to the regulation formulated by the district heating service provider, the DH system of Chifeng can only operate six months (October to April the next year) every year. A considerable amount of heat was released into the environment during the non-heating season. Therefore, in 2016, the construction of an STES and solar thermal systems started as part of a pilot project that aimed to exploit the full potential of the waste heat from Jinjian Copper Plant. Fig. 1 shows the position of each system components for the pilot project. The excess heat from the copper plant still serves as the main heating supply source. Three hundred and thirty-six solar thermal collector panels with a total effective area of 1002 m^2 represent another heat source, which contributes 0.42 GWh on annual heating production. A borehole thermal energy storage with a volume of 0.5 million m^3 is located directly below the solar field. A dedicated machine room is located next to the storage body containing all the mechanical equipment, i.e. heat exchangers, pumps, valves, control system and auxiliary components. The project has completed the construction phase and is currently under trial operation.

2.1. System configuration

As the recovered industrial waste heat (IWH) serves both the internal and external district heating networks, there are two options for applying the pilot system. Fig. 2 shows the system diagrams for the two system configurations in both the heating season and the non-heating season. Different system components have separate circuits and connect to the system circulation loop through heat exchangers. The design circulation flow rate is 30 m^3/h all year round. The heat carrier in the circulation loop is hot water. In the non-heating season (15th of April to 15th of October), water is heated to 70 °C by the waste heat recovery system (IWH1) and further raised to 75 °C by the solar thermal system. The hot water then flows through the STES system, injecting heat into the storage. The circulated water reaches around 50 °C after releasing heat to the soil and then flows back to the waste heat recovery system.

From the 16th of October to the 14th of April the following year, the system switches to the heating season operation mode. The low-temperature water from the end-users first exchanges heat with the thermal energy extracted from the STES. The circulated water is then heated by the solar thermal system, which on average results in approximately 5 °C of temperature increase. According to the types of end-users, two system configurations can be selected, i.e. an internal heating network for the Copper plant (System1), and as a component of the external district heating network serving Chifeng City (System2). The difference between the two configurations is the return temperature from the district heating network. The temperature defines the lowest temperature level in the district heating system and is used to discharge the

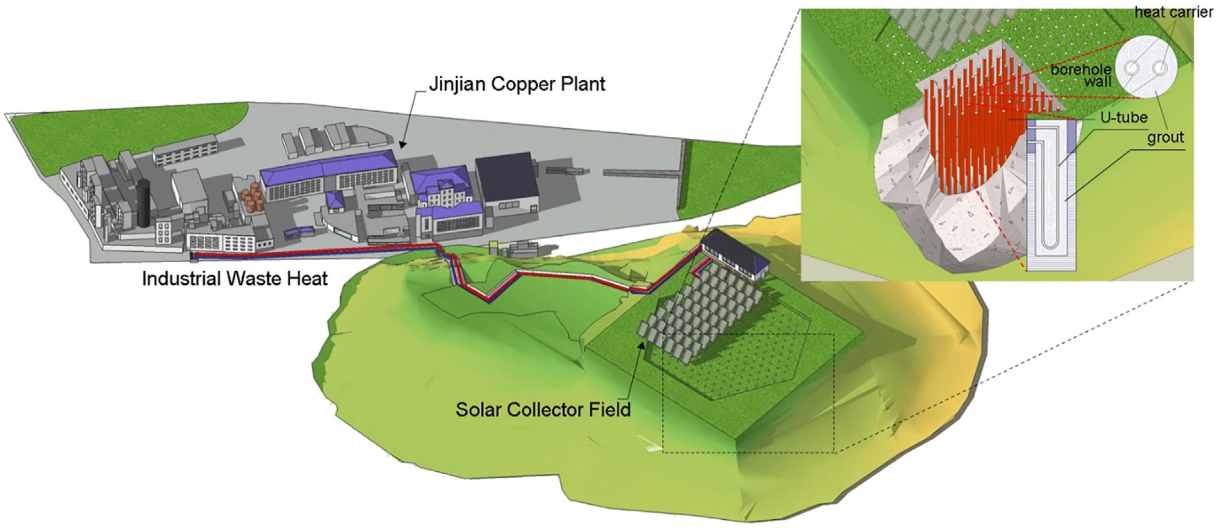

Fig. 1. Design sketch of the project.

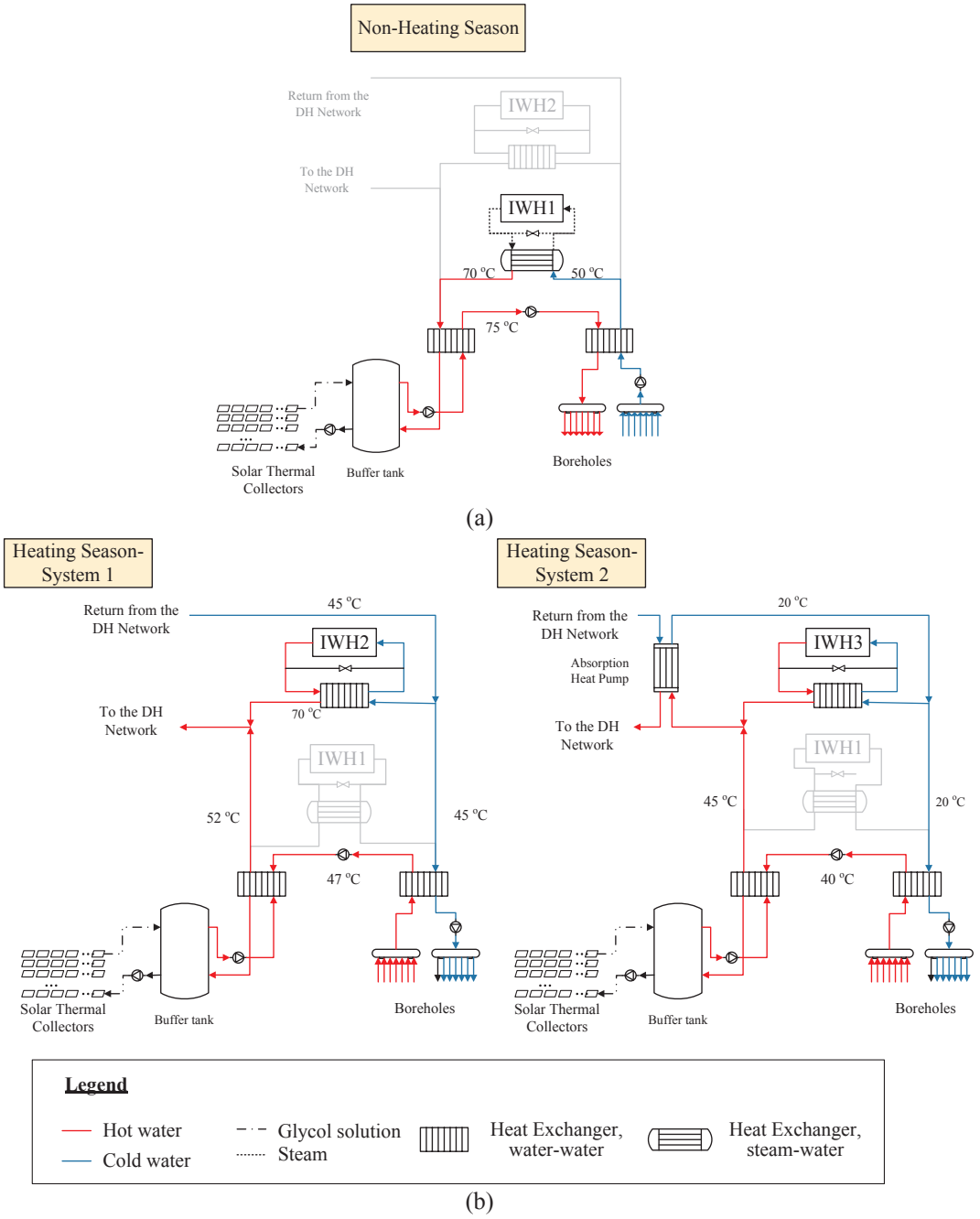

Fig. 2. System diagram under desired operational condition for (a) non-heating season and (b) heating season.

STES. The internal district heating network feeds in the return water from the buildings directly to the heat exchanger in the circulation loop. The water temperature ranges from 45 to 55 °C. An excess heat recovery system (IWH2) acts as a back-up heating source. The return water of system 2 comes from the substation equipped with an absorption heat pump. The absorption heat pump is essentially a water source heat pump driven by the heated water instead of electricity. Its principle of operation based on the absorption and evaporation of an absorption medium. In this pilot system, the absorption heat pump recycles heat from low temperature recovered excess heat from the copper plant (IWH3) and solar thermal system, to produce high-temperature water for the DH system. The low-temperature water is cooled to a very low water temperature at around 20 °C.

2.2. The seasonal thermal energy storage

The borehole thermal energy storage in the pilot case study consists of 468 boreholes in total. Each borehole contains an eighty-meter-deep single-U tube heat exchanger. The distance between every two boreholes is four meters, measured from the center of the borehole. The borehole field covers an area of 96 m in diameter. In order to minimize heat losses to the surrounding soil and for the convenience of construction, the borehole thermal energy storage adopts a hexahedron shape to arrange the borehole heat exchangers, as shown in Fig. 3. The whole storage is divided into six subzones for purposes of monitoring and control. At the surface, six borehole heat exchangers are connected in series to a branch, and thirteen branches are connected in parallel in

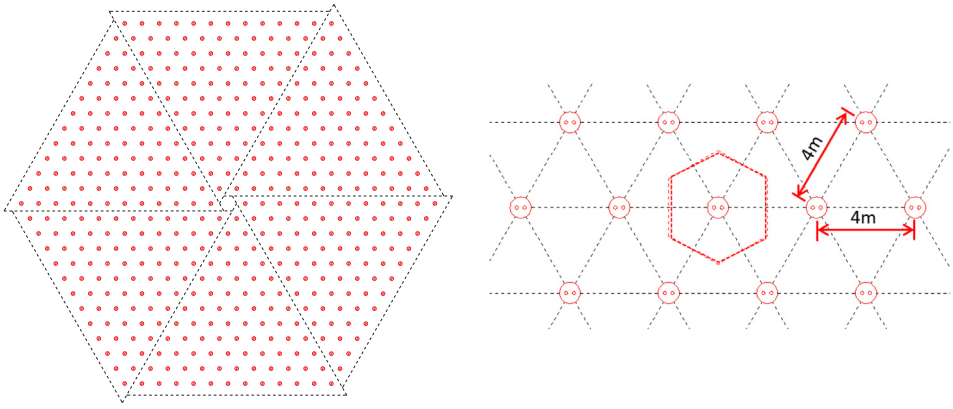

Fig. 3. Aerial view of the borehole field.

each subzone. The length of the pipe branches in one subzone is similar to each other to maintain hydraulic balance. The 78-branch U-tube heat exchangers are joined together in six groups at the ground surface and then connect back to the machine room.

3. The model-based approach for the STES system performance assessment

Modeling and simulations are executed in Dymola (version 2016 FD01), a commercial modeling and simulation environment based on the Modelica language. Modeling and simulation approaches for the main components, including the building thermal model, industrial waste heat, solar thermal system and seasonal thermal storage, are described below. The validity of models for the main components is also included.

3.1. Model description

3.1.1. Solar thermal system model

The buffer tank is modeled by a stratified water tank model from the *Buildings* Library (Buildings.Fluid.Storage.StratifiedEnhancedInternalHex) with a heat exchanger inside the tank. The tank model is discretized into four segments for the vertical dimension. Heat conduction through the top and side of the tank with the ambient temperature at a constant 20 °C is calculated in the model. A temperature sensor is placed at the bottom segment in the tank model to monitor the temperature difference between the buffer tank and inlet temperature in the system circulation loop. When the pump between the tank and the circulation heat exchanger is operating and the temperature difference is smaller than 1 °C, the pump will stop. It will start to operate again when the temperature difference is larger than 5 °C. The solar collector model (Buildings.Fluid.SolarCollectors.ASHRAE93) was built according to the ASHRAE93 test standard [18]. All the technical data is taken from the Solar Rating and Certification Corporation (SRCC) website. For each solar panel, the model discretizes the solar collector volume into i segments. Here i = 3 which was the minimum number required by the solar collector model. Fig. 4 shows the energy balance of one solar panel. In the buffer tank model and the solar collector model, dynamic equations are applied to solve the mass balance and the energy balance. The tank model and the solar collector model have been validated by their developers as stated in the Modelica Buildings Library Documentation [19].

3.1.2. Seasonal thermal energy storage system model

Based on the need to assess the energy performance of the underground STES, as illustrated in Section 1.3, this study chose the HSRM to model the seasonal borehole thermal energy storage. The model combines a short-term thermal response model with a long-term thermal response model. The short-term thermal response model adopts Bauer et al.'s thermal resistive-capacitive models [20] for coaxial, single- and double-U-tube. The structure of the short-term model is shown in Fig. 5. The short-term model calculates the transient thermal response of the heat carrier fluid, the grout, and the surrounding ground accurately for a short time period. The time period ranges from minutes to $t = 5r_b^2/\alpha$, where r_b represents the radius of a borehole and α is the ground thermal diffusivity. The analytical model proposed by Claesson and Javed [21] is adopted to calculate the long-term thermal response in the HSRM. The short-term and long-term thermal response models have been validated by the model developers. The short-term thermal response model was compared to the widely used sandbox experiment [22] and the DST model (type 557a in TRNSYS). TRNSYS DST model and the HSRM model gave similar results. The relative error between the simulated result from the HSRM model and the sandbox experiment was 1.7% [14]. The long-term thermal response model is verified using the well-known g-function developed by Eskilson [23] and the infinite cylindrical heat source (CHS) solution [24] for different configurations. The implementation of the HSRM in Modelica is the *MultipleBoreHolesUTube* model from the *IDEAS* library. The exact coordinates of the 468 boreholes, as shown in Fig. 3, were inputted into the model. Since the *MultipleBoreHolesUTube* model assumes heat carrier flows through every borehole heat exchanger in parallel, this study connected six *MultipleBoreHolesUTube* model blocks to represent the system design. To maintain the horizontal temperature stratification in the borehole thermal energy storage, this study switches the flow direction in the STES system circuit when system operation moves from the heating season to the non-heating season and vice versa.

3.1.3. Building thermal model

Building thermal demands are modeled by a lumped element model of an equivalent electric circuit (also known as thermal network model). As shown in Fig. 6, one resistance (R) represents the heat conduction through the building envelope. A single capacitance C represents the thermal mass of the building. Heat transfer by infiltration is reflected by UA. Solar and internal heat gains (Q_{solar} and Q_{int} respectively) are connected to the indoor air temperature node T_{in}. Q_{dem} is the amount of heating demand to be supplied to the indoor air temperature node. It is calculated through the radiator model *RadiatorEN442_2* from the *Buildings* library (version 3.0.0). The model is validated by comparing the calculated peak heating load to the corresponding design figures of the DH system according to a previous study [25].

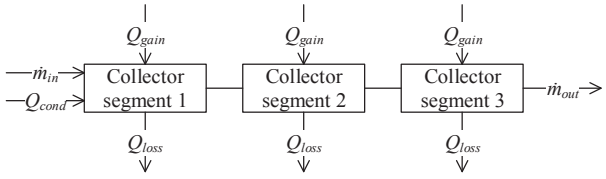

Fig. 4. Schematic overview of the nodal energy balance in one solar panel.

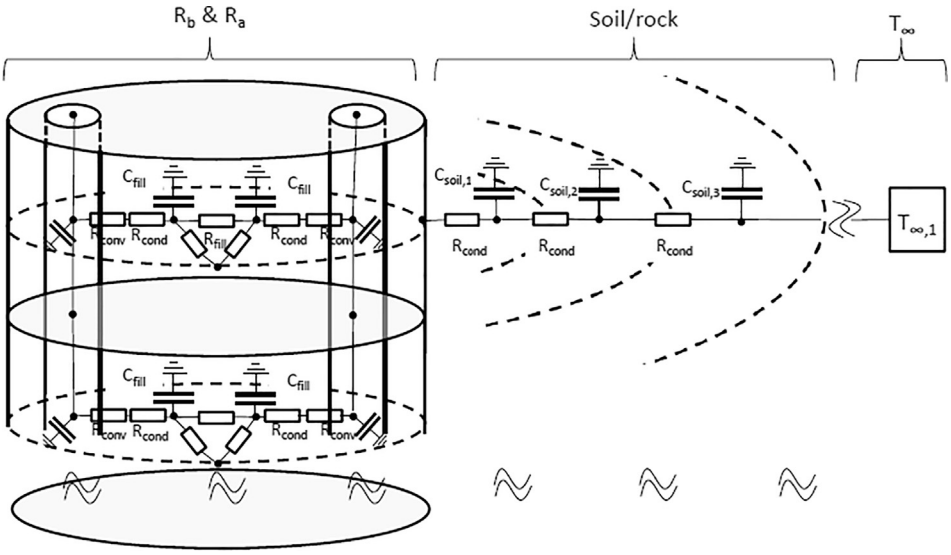

Fig. 5. Structure of the short-term model for a single borehole with a single-U-tube configuration [14]

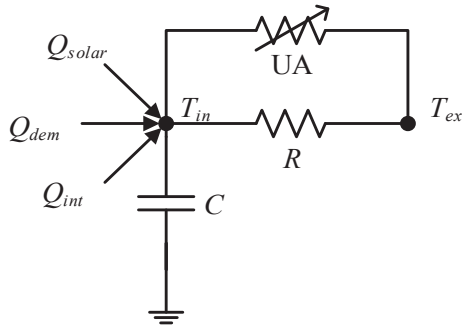

Fig. 6. Schematic of the building thermal network model.

In this study, thermal characteristics of different elements used in building heating demand simulation refer to the definition of the baseline building in the Design Standard for Energy Efficiency of Public Buildings (GB50189-2005). U-values for external wall/floor, roof and window are 1.28 W/(m^2·K), 0.77 W/(m^2·K) and 3.26 W/(m^2·K) respectively. These thermal characteristics reflect a typical building constructed in the 1980s in the same climate zone.

3.1.4. Industrial waste heat model

This study uses a heat exchanger with a controlled hot water supply to represent the industrial waste heat. The heat transfer from the acid to the water is omitted. The reason for the simplification is that the excess heat source from the copper plant is relatively stable. Therefore, on one side of the heat exchanger, a mass flow source supplied 70 °C hot water at a constant flow rate. The heat transfer through the heat exchanger is calculated as follows:

$$Q = Q_{max} \cdot \varepsilon \quad (1)$$

where ε is a constant effectiveness and Q_{max} is the maximum heat that can be transferred. Q_{max} is calculated as:

$$Q_{max} = min(c_{p1} m_{f1}, c_{p2} m_{f2}) \cdot (T_{inl2} - T_{inl1}) \quad (2)$$

where m_{f1} and m_{f2} are the mass flow rates of the two sides of the heat exchanger, c_{p1} and c_{p2} are the specific heat capacity of the fluid in the two sides of the heat exchanger, T_{inl1} and T_{inl2} are the inlet temperature of the fluid in the two sides of the heat exchanger. Here defined side 2 connected to the heat source. Therefore, T_{inl2} = 70 °C.

A by-pass is added to make sure supply temperature for space heating is 60 ± 1 °C using an on/off control valve. The other side of the heat exchanger (side 1) is connected directly to the distribution network.

3.2. Simulation setup

To assess the performance of the underground STES for the presented case study, this research designed the following computational experiments. D1 and D2 represent the computational experiments for the two system configurations under the design conditions. The weather file used for simulating building demand and solar thermal energy is the Chinese Standard Weather Data (CSWD) in Chifeng. Industrial waste heat is simulated as a constant mass flow source at 70 °C. The demand for the copper plant heating network case (D1) is simulated by the building thermal model described in the previous section. Since the return water in the Chifeng city heating network case (D2) comes from the absorption heat pump at a relatively stable temperature level of 25 °C, the demand is modeled as a constant mass flow source.

In addition, this study also conducts computational experiments to analyze the impact of site parameters on the performance of the underground STES. Eight cases are conducted to investigate the local sensitivities of thermal conductivity and specific heat capacity of the grout material and the soil. Table 1 presents the ID and a short description for each computational experiment. The design parameters of the grout material and the soil are listed in Table 2.

Table 1
Description of the investigated computational experiments.

ID	Remarks
D1	Designed performance assessment for the copper plant heating network (internal)
D2	Designed performance assessment for the Chifeng city heating network case (external)
G_k + 10	Thermal conductivity of the grout material is 10% bigger than designed
G_k − 10	Thermal conductivity of the grout material is 10% smaller than designed
G_c + 10	Specific heat capacity of the grout material is 10% bigger than designed
G_c − 10	Specific heat capacity of the grout material is 10% smaller than designed
S_k + 10	Thermal conductivity of the soil is 10% bigger than designed
S_k − 10	Thermal conductivity of the soil is 10% smaller than designed
S_c + 10	Specific heat capacity of the soil is 10% bigger than designed
S_c − 10	Specific heat capacity of the soil is 10% smaller than designed

3.3. Performance indicators selection

Based on the overview of the performance indicators presented in Section 1.3, this study chose the Extraction Heat Q_{ext}, the Injection Heat Q_{inj} and the Storage Coefficient S to assess the annual energy performance of the STES. The transient thermal behavior of the STES is demonstrated by the hourly heating flow through the STES and by the stabilization time t_s in years. The stabilization time t_s is calculated by comparing the mean temperature difference of the water leaving the STES in the non-heating season between two adjacent operation years. When the mean temperature difference is lower than a certain threshold ΔT_{ref}, then the STES is considered to reach a normal operational condition.

As for the sensitivity analysis, the sensitivity of the site parameters listed in Table 2 is evaluated by the point elasticity method. Eq. (3) defines the Influence Coefficient (IC) as the ratio of the output and the input [26]. IP and OP in Eq. (3) represent the values of inputs and outputs respectively. OP_B and IP_B are the reference values of inputs and outputs for the design condition. Since the values of inputs can be either larger or smaller than the reference values, two values of IC for each parameter are obtained and the performance indicator for sensitivity of each parameter is the average influence coefficient.

$$IC = \left| \frac{\frac{OP - OP_B}{OP_B}}{\frac{IP - IP_B}{IP_B}} \right| \tag{3}$$

4. Simulation results for the STES system energy performance

4.1. Simulated energy performance under the design condition

This research conducted computational experiments on the utilization of the underground STES in the two system configurations, i.e. connecting to the copper plant internal heating network (D1) and joining the Chifeng city heating network (D2). Both cases are evaluated at the desired operational conditions after the stabilization period. The annual energy performance of the STES for D1 and D2 are shown in Table 3. Comparing the two designs, the extraction heat for the Chifeng city heating network application is five times higher than that of the copper plant internal heating network. Similar phenomenon can be observed for the annual injection heat and the storage coefficient. The energy performance of the underground STES is better in the case of the Chifeng city heating network application.

The reason for the discrepancy can be explained by the difference in the inlet water temperature T_r (position refers to Fig. 7), which mainly defines the amount of heat when discharging the STES. Fig. 8 shows the hourly distribution of the T_r for the two designs. The top and bottom of the blue box in Fig. 8 are the 25% and 75% of the hourly T_r data set. The red line represents the median value of the hourly distribution data. The black lines extended above and below the blue box show the maximum and the minimum value of the hourly distribution data. As designed, the inlet water temperature for D2 was 25 °C, whereas the T_r for D1 varies from 48.1 °C to 59.9 °C with a median value of 51.9 °C. The relatively high value of inlet water temperature was similar to the temperature level in the STES. Therefore, both extraction heat and injection heat for the copper plant internal heating network case were much lower than for the other case.

Fig. 9 illustrates the hourly distribution of the heat injected in and extracted from the STES for D1 and D2 respectively. The boxplots in Fig. 9 share the same definition as in Fig. 8. Positive values for the hourly heating flow represent heat injection into the STES, whereas negative values represent heat extraction. During the heating season, although the system was designed to extract heating from the STES, the STES still stored heat for more than 25% of the time due to high inlet temperatures, T_r, in the case of connecting to the copper plant internal heating network (D1). The total extracted heat for the case D2 was three times larger than D1. The extra heat supplied by the industrial waste heat for case D2 was 44% less than in case D1.

4.2. Impact of site parameters on the STES system energy performance

The impact of site parameters on the STES system energy performance is evaluated according to the influence coefficient through sensitivity analysis. The influence coefficient is a dimensionless indicator reflecting the relationship between the variation in output and input. This research considered four input parameters, namely the thermal conductivity and the specific heat capacity of the grout material and the soil. Outputs are the annual extraction heat, the injection heat and the storage coefficient. Taking the transient thermal behavior into consideration, each output is examined under initial operational conditions during the first year and under stable operational conditions during the tenth year. Table 4 lists the influence coefficient for the selected performance indicators.

For the case of the grout material properties, the influence of the specific heat capacity on the injected heat was slightly larger than the influence of the thermal conductivity, while the situation for the extracted heat and the storage coefficient was vice versa. Comparing the initial and stable operations, most of the IC values under stable operational conditions were much smaller than those under initial operational conditions, except for the IC of specific heat capacity for the extracted heat. However, all the IC values of the gout material properties were very small. The maximum IC of grout material properties was only 0.056.

As for thermal properties of the soil, the influence of the variation of input parameters is much more significant. The IC value ranged from 0.044 to 1.239. This represents 0.4% to 12.4% variance on the chosen performance indicators. The most sensitive input parameters for each performance indicators are specific heat capacity for the heat extraction in initial operational conditions, and thermal conductivity for the injected heat and the storage coefficient in stable operational conditions.

5. Discussion on the long-term performance of STES systems

To assess the energy performance of the STES system under design conditions, this research conducted long-term simulations to obtain the stabilization time t_s. As described in Section 3.3, the stabilization time t_s is obtained by comparing the outlet temperature in the heating season between the adjacent two years to a defined temperature threshold ΔT_{ref}. To better understand how the system gradually achieves the stabilization status, the hourly outlet temperature of the STES with a 25 °C input temperature in the heating season for the first ten years operation is plotted, as shown in Fig. 10. Numbers on the x-axis are the hours in a heating season. Zero represents the start of each heating season. Each line represents an hourly outlet temperature profile of a whole heating season. The blue line at the bottom is the temperature profile of the first heating season. The orange line at the top is the temperature profile of the tenth heating season. All the heating seasons of the second year to the ninth year lie in between. In general, all the outlet water temperature profiles show a steady drop from the start to the end of a heating season. Comparing the difference between years, the outlet water temperature of the STES in the beginning of a heating season is always higher than the previous heating season. The reason of the difference is that, as the system operation goes on, heat is kept

Table 2
Thermal properties of the grout material and the soil.

	Thermal conductivity, k W/(m·K)	Specific heat capacity, c J/(kg·K)	Density, d kg/m^3
Grout	2.2	800	1600
Soil	0.852	1103	1500

Table 3
Annual energy performance of the STES system for D1 and D2.

ID	Extraction heat Q_{ext} (GWh)	Injection heat Q_{inj} (GWh)	Storage coefficient S
D1	0.35	2.14	16.4%
D2	2.17	3.29	65.9%

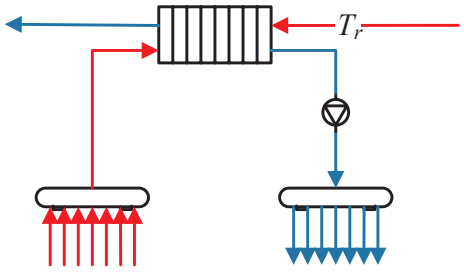

Fig. 7. The schematic diagram of the STES system circuit.

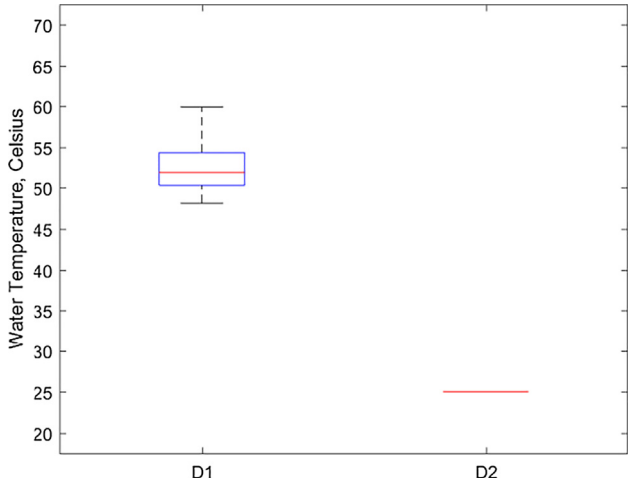

Fig. 8. Hourly distribution of the inlet water temperature T_r for D1 and D2 during the heating season.

injecting into the storage every year thus soil temperature increases in the storage. However, the differences between the adjacent two years gradually decreased as the operation continues. The descending differences indicate that the system is reaching the stabilization status.

Fig. 11 shows the hourly distribution of the outlet temperature difference in the heating season at different inlet temperatures, ranging from 25 to 55 °C. Each box represents the hourly distribution of the outlet temperature difference between the heating seasons of two adjacent years. The boxplots in Fig. 11 share the same definition as in Fig. 8. Take the top-left graph in Fig. 11 as an example, the first box consists the hourly differences between the first heating season and the second heating season, i.e. the distance between the bottom line profile (the blue line) and the second bottom line profile (the dark orange line) as shown in Fig. 10. During system operation, the mean temperature difference and the distribution range for each year decreased. The mean temperature difference is observed to be smaller than 1 °C after the second year for the case with T_r = 25 °C and after the third year for the other three cases. Therefore, the stabilization time values for the four cases are 2, 3, 3, 3 years when ΔT_{ref} = 1. If ΔT_{ref} = 0.5, the stabilization times for the four cases are 3, 4, 4, 4. If ΔT_{ref} is further lower to 0.1, the values will be 9, 10, 10, 11. Obviously, the higher the ΔT_{ref} is, the shorter the t_s will be.

There are mainly two utilizations of the t_s. Firstly, as used in this study, to obtain the stable status of the STES. Then the temperature field at the stable status can be used to initialize the STES to further assess the energy performance of the STES system under design conditions. Finally, and even more practical in industrial projects, it can help the designers to understand how long it will take to achieve the desired operational status for the underground STES under different design parameters. In this case, more scenarios need to be taken into consideration, and it is the designer's choice to decide the value of the temperature thresholds.

6. Conclusion

This research proposed a model-based method to assess the energy performance of underground STES and applied it to a case study of a pilot DH system in Chifeng, China. The research adopted Modelica models from open source libraries to evaluate such systems. The results show that the STES improved its performance when connected to the Chifeng city district heating network. Here, the stored heat was three times higher than in the case where the STES was connected to the

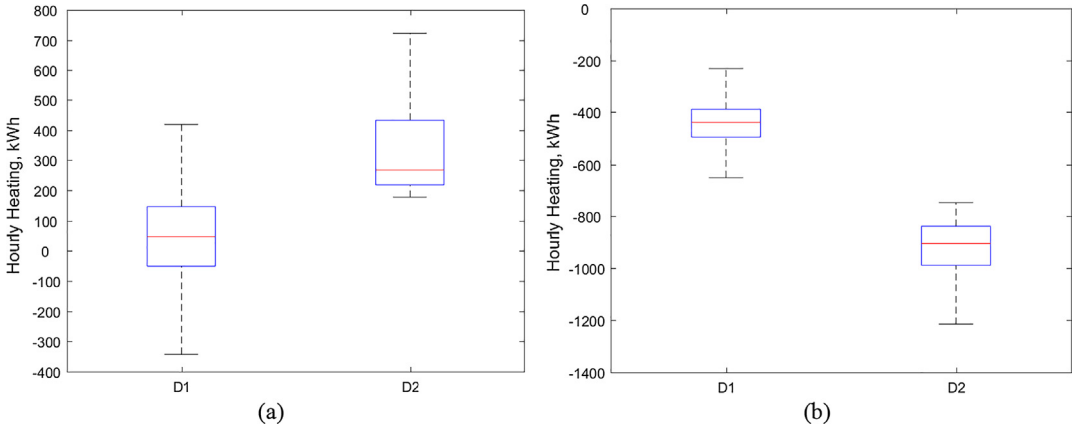

Fig. 9. Hourly heat injection and extraction distribution for D1 and D2 during the heating season (a) and the non-heating seasons (b), positive values represent heat injection and negative values represent heat extraction.

Table 4
Influence coefficient of properties of the grout material for the STES system performance.

Input parameters	IC for the heat extraction		IC for the heat injection		IC for the storage coefficient	
	Initial operation	Stable operation	Initial operation	Stable operation	Initial operation	Stable operation
Thermal conductivity of the grout material, k_g	0.080	0.043	0.024	3.11e-04	0.058	0.014
Specific heat capacity of the grout material, c_g	0.0017	0.0018	0.029	6.18e-04	0.0012	3.08e-04
Thermal conductivity of the soil, k_s	0.874	0.434	0.388	0.527	0.464	1.239
Specific heat capacity of the soil, c_s	0.992	0.060	0.206	0.044	0.093	0.103

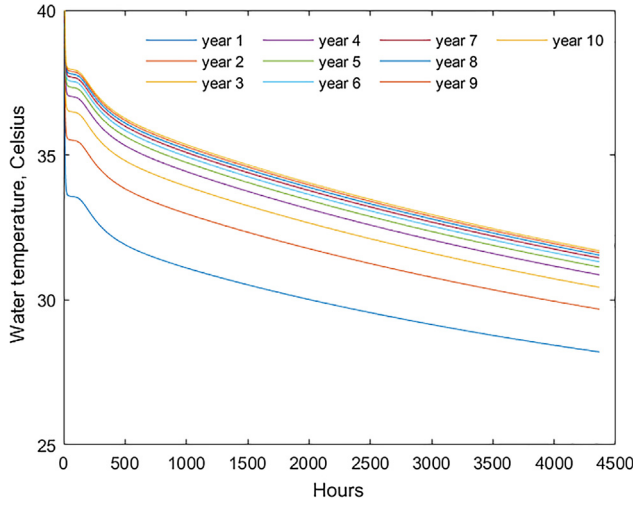

Fig. 10. Hourly outlet temperature of the STES with a 25 °C input temperature in the heating season.

copper plant's internal heating network. In the case of Chifeng, the lower temperature input required to discharge the underground STES helped to achieve a higher storage coefficient and a shorter stabilization time between one and two years.

The impact of site parameters on the STES system performance was evaluated through a sensitivity study. In general, soil thermal conductivity is the most sensitive parameter in terms of STES system performance. The greatest influence was caused by the thermal conductivity of the soil on the storage coefficient in stable conditions, which increased or decreased by 12.4%. The thermal conductivity of both the grout material and the soil influenced the STES system performance more than the specific heat capacity. Therefore, the data quality of these sensitive inputs require special attention.

Last but not least, it is crucial to evaluate the energy performance of underground STES systems over a long-term period of at least three years. Future work will focus on detailed analysis of different scenarios and quantify the corresponding uncertainty in order to achieve a better design.

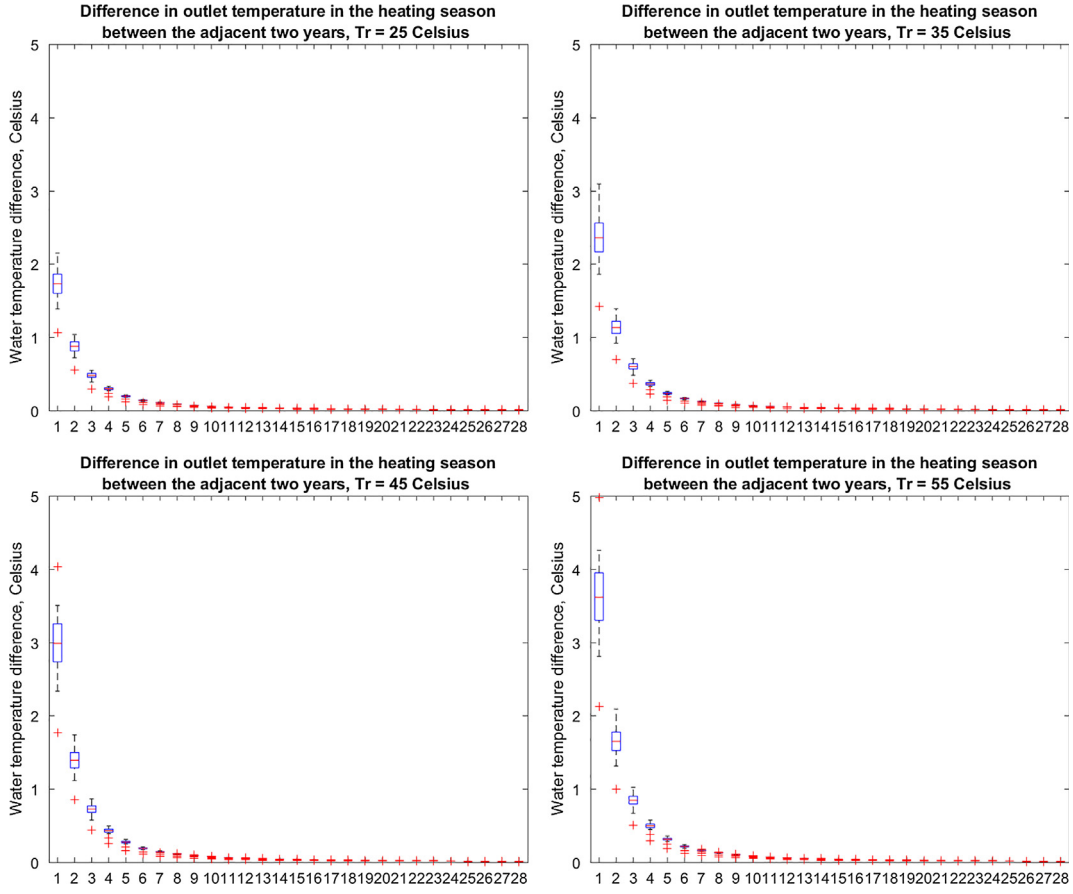

Fig. 11. Distribution of the outlet temperature difference in the heating season at different input temperature levels.

Acknowledgements

This research is part of the seasonal storage for solar and industrial waste heat utilization for urban district heating project funded by the Joint Scientific Thematic Research Programme (JSTP) – Smart Energy in Smart Cities. We gratefully acknowledge the financial support from the Netherlands Organisation for Scientific Research (NWO). We would also like to thank our research partners from Tsinghua University working on the project of the International S&T Cooperation Program of China (ISTCP) (project No. 2015DFG62410). Without their efforts, we would not have been able to obtain the technical data to conduct the case study.

References

[1] National Bureau of Statistics of China, China Statistic Year Book 2015, China Statistic Press, 2015.
[2] National Development and Reform Commission, The 13th Five-Year Plan on Renewable Energy Development, National Development and Reform Commission (NDRC), 2016.
[3] H. Lund, S. Werner, R. Wiltshire, S. Svendsen, J.E. Thorsen, F. Hvelplund, et al., 4th Generation District Heating (4GDH): Integrating smart thermal grids into future sustainable energy systems, Energy 68 (2014) 1–11.
[4] O. Odgaard, China's Quest for New District Heating Reforms, ThinkChina, Copenhagen, Denmark, 2015.
[5] M. Gong, S. Werner, District Heating Research in China, Svensk Fjärrvärme AB, Stockholm, Sweden, 2014.
[6] Ministry of Housing and Urban-Rural Development of China, Design Standard for Energy Efficiency of Residential Buildings in Severe Cold and Cold Zones, China Architecture Industry Press, Beijing, 2010.
[7] H. Gadd, S. Werner, Achieving low return temperatures from district heating substations, Appl. Energy 136 (2014) 59–67.
[8] P.D. Thomsen, P.M. Overbye, Energy storage for district energy systems, in: R. Wiltshire (Ed.), Advanced District Heating and Cooling (DHC) Systems, (2016), Woodhead Publishing; Oxford, pp. 145–166.
[9] M. Philippe, D. Marchio, S. Hagspiel, P. Riederer, V. Partenay, Analysis of 30 underground thermal energy storage systems for building heating and cooling and district heating, in: The 11th International Conference on Thermal Energy Storage. Stockholm, (200p), pp. 1–8.
[10] T. Schmidt, O. Miedaner, Solar district heating guidelines: Storage Fact sheet 7.2 [Internet]. Stuttgart, Germany, 2012 [cited 2017 Feb 10]. Available from: http://solar-district-heating.eu/Portals/0/Factsheets/SDH-WP3_FS-7-2_Storage_version3.pdf.
[11] P. Eskilson, J. Claesson, Simulation model for thermally interacting heat extraction boreholes, Numer. Heat Transf. 13 (2) (1988 Mar) 149–165.
[12] C. Yavuzturk, J.D. Spitler, A short time step response factor model for vertical ground loop heat exchangers, ASHRAE Trans. 105 (2) (1999) 475–485.
[13] HellstrÄom Gä, Heat Storage in the Ground Duct Ground Heat Storage Model, Manual for Computer Code, University of Lund, Lund, Sweden, 1989.
[14] D. Picard, L. Helsen, A new hybrid model for borefield heat exchangers performance evaluation, in: Proc 10th Int Model Conf., 2014, pp. 857–866.
[15] B. Sibbitt, D. Mcclenahan, R. Djebbar, J. Thornton, B. Wong, J. Carriere, et al. Measured and simulated performance of a high solar fraction district heating system with seasonal storage, in: Proc 30th Ises Bienn Sol World Congr 2011, Swc 2011, 2011, pp. 3037–3048.
[16] D.O. Schulte, W. Rühaak, S. Oladyshkin, B. Welsch, I. Sass, Optimization of medium-deep borehole thermal energy storage systems, Energy Technol. 4 (2016) 104–113.
[17] S. Lanini, F. Delaleux, X. Py, R. Olivès, D. Nguyen, Improvement of borehole thermal energy storage design based on experimental and modelling results, Energy Build. 77 (2014) 393–400.
[18] ASHRAE. ASHRAE Standard 93-2010, Methods of Testing to Determine the Thermal Performance of Solar Collectors, American Society of Heating, Refrigerating & Air Conditioning Engineers, 2010.
[19] M. Wetter, W. Zuo, T.S. Nouidui, X. Pang, Modelica buildings library, J. Build. Perform. Simul. 7 (4) (2014) 253–270.
[20] D. Bauer, W. Heidemann, H. Müller-Steinhagen, H.-J.J.G. Diersch, Thermal resistance and capacity models for borehole heat exchangers, Int. J. Energy Res. 35 (4) (2011) 312–320.
[21] J. Claesson, S. Javed, An analytical method to calculate borehole fluid temperatures for time-scales from minutes to decades, ASHRAE Trans. 117 (PART 2) (2011) 279–288.
[22] R.A. Beier, M.D. Smith, J.D. Spitler, Reference data sets for vertical borehole ground heat exchanger models and thermal response test analysis, Geothermics 40 (1) (2011) 79–85.
[23] P. Eskilson, Thermal analysis of heat extraction boreholes, Response (1987) 222.
[24] H.S. Carslaw, J.C. Jaeger, Conduction of Heat in Solids, second ed., Clarendon Press, Oxford, 1959.
[25] L. Xu, J.I. Torrens, J.L.M. Hensen, Comparison of two simulation methods for the technical feasibility of a district heating system using waste heat from a copper plant with thermal storage, in: C.S. Barnaby and M. Wetter (Eds.), Proceedings of the International Building Performance Simulation Association Building Simulation Conference, IBPSA, San Francisco, 2017, pp. 940–948.
[26] J.C. Lam, S.C.M. Hui, Sensitivity analysis of energy performance of office buildings, Build Environ. 31 (1) (1996) 27–39.